# THE EFFECT OF GAS PUFFING AT THE LH GRILL ON THE EFFICIENCY OF THE CENTRAL DENSE PLASMA ION HEATING AT THE FT-2 TOKAMAK

D.V. KOUPRIENKO, A.B. ALTUKHOV, D.YU. BATYREV, M.V. DERYABINA, V.V. DYACHENKO, L.A. ESIPOV, A.D. GURCHENKO, E.Z. GUSAKOV, M.A. IRZAK, M.YU. KANTOR, E.O. KISELEV, A.N. KONOVALOV, S.I. LASHKUL, A.YU. POPOV, S.V. SHATALIN

**Ioffe Institute** 

St. Petersburg, Russian Federation Email: denis.kouprienko@mail.ioffe.ru

#### Abstract

The paper presents recent results of central dense plasma lower hybrid (LH) ion heating experiments at the FT-2 tokamak. Variation of the gas puffing valves versus LH grill position is applied, performing different ion heating efficiency. The formation of a strongly non-monotonic density profile is observed during LH pulse. Two mechanisms are discussed as potential causes of this effect: the influence of ponderomotive forces and the emergence of an ITB (Internal Transport Barrier).

#### 1. INTRODUCTION

Additional heating of plasma ion component using radio-frequency (RF) waves in the lower hybrid (LH) frequency range was actively developed in the late 1970s. However, its application in small tokamaks did not perform relevant positive results [1] and therefore it was not tested at large machines. The efficiency of this heating method depends on numerous parameters, including the constructive arrangement of the RF antenna relative to the neutral gas source. This paper describes an effective LH heating (LHH) scenario for high-density deuterium plasma  $\langle n_e \rangle_{OH} \ge 5 \cdot 10^{19} \text{m}^{-3}$  [2], presenting experimental results on heating with varying arrangements of the gas puffing valves versus LH grill position. High efficiency of central ion heating is observed, which depends significantly on these arrangements. Additionally, the LHH scenario with gas puffing in front of the grill shows plasma displacement from the RF antenna, that grows with the RF power. This phenomenon is attributed to the ponderomotive mechanism of interaction between LH wave and plasma. Furthermore, the formation of a nonmonotonic plasma density profile is observed, supposing the formation of an internal transport barrier (ITB).

## EXPERIMENTAL APPROACH

In this paper we perform high-density deuterium discharges in the FT-2 tokamak (a = 0.08m, R = 0.55m,  $30\text{kA} < I_{pl} < 35 \text{ kA}$ ,  $2\text{T} < B_T < 2.3\text{T}$ ,  $q_{95} \sim 3-4$ ;  $\langle n_e \rangle \sim (5-7) \cdot 10^{19} \text{ m}^{-3}$ ). The effect of pulsed gas puffing on the efficiency of additional central Lower Hybrid Ion Heating (LHH) in dense plasma is studied. Two discharge scenarios were compared: gas puffing in front of the LH grill position (valve PV2) versus gas puffing in neighboring sections (valve PV1 and PV3), toroidally shifted by  $\pm \pi/2$  relative to the PV2 valve.

In the later scenario application of LH heating ( $t_{LH} = 28-25$  ms,  $P_{LHH} = 100$  kW,  $f_{LH} = 920$  MHz) resulted in central ion heating  $T_{i cent}$  from 200eV up to 350 eV, measured by Nuclear Particle Analyzer, (NPA), see Fig. 1.

#112323D

500

400

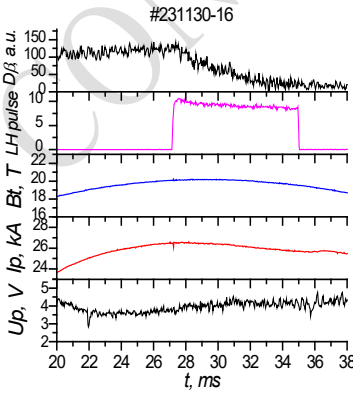
200

e< 300 PV1 OH 27ms

-PV2 OH 27ms

-PV1 LHH 33ms

PV2 LHH 33ms



Loop voltage Up, plasma current Ip,

toroidal field Bt, LH pulse and  $D_{\beta}$ 

line emission

Fig. 1a. LHH discharge scenario.

100 0 0 2 5 6 3 4 r. cm Fig. 1b. Ion temperature: comparison of ion heating at pulsed gas puffing via

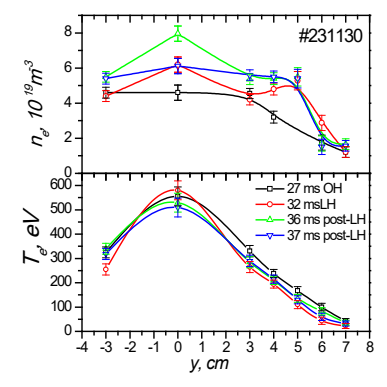


Fig. 1c. PV2 case.  $T_e(r)$  and  $n_e(r)$  profiles during LHH: valves PV1 and PV2 ohmic, LH and post-LH stages

Thomson scattering (TS) profiles indicated a density increase with slight peaking of the electron temperature  $T_e(r)$ . The formation of a  $\Pi$ -shaped density profile with a steep density gradient at the plasma periphery was accompanied by a reduction in  $D_{\beta}$  line emission.

The first scenario was performed under the same plasma parameters with gas puffing in the vicinity of the grill antenna aperture (PV2). More efficient additional ion heating was observed here with  $T_{i cent}$  increasing from 200 eV up to 450 eV (see Fig. 1b). Notably, in the PV2 case in both the lower hybrid current drive (LHCD) mode and ion heating (LHH) mode the suppression of parametric decay instability (PDI) was observed [3,4].

Effective ion heating in the PV2 case is accompanied by significant distortion of the density profiles measured by Thomson scattering (TS). During LH pulse these profiles became non-monotonic at mid-radii ( $r = \pm 4-5$  cm,  $q \approx 2$ ), presenting density "ears" and an additional secondary maximum formation (Fig. 1c). The origin of this effect is discussed below.

#### 3. RECONSTRUCTION OF MAGNETIC CONFIGURATION

Non-monotonic density profiles demand special procedure to reconstruct magnetic surfaces, based on the reconstruction of local density [5]. This procedure was applied for discharge #301123, PV2 case, with plasma current of 28kA, toroidal magnetic field of 2.1T and average density ranging from  $5.5 \cdot 10^{19} \text{m}^{-3}$  to  $6.9 \cdot 10^{19} \text{m}^{-3}$ . The calculations were performed for 27 (OH stage), 32 (LHH stage), 36 and 37 ms (post-LHH stage). Fig. 2 shows the plasma boundary (a) for each of these time periods, as well as the chord of the interferometer represented by black vertical lines. The points measured by Thomson scattering (TS) diagnostics are marked with black dots (probing vertical chord at R = 56.5 cm), along with the electron density points, experimental data points of the interferometer phase and height, and the displacement of the observation chord relative to the large radius of the vessel ( $R_0 = 55 \text{ cm}$ ).

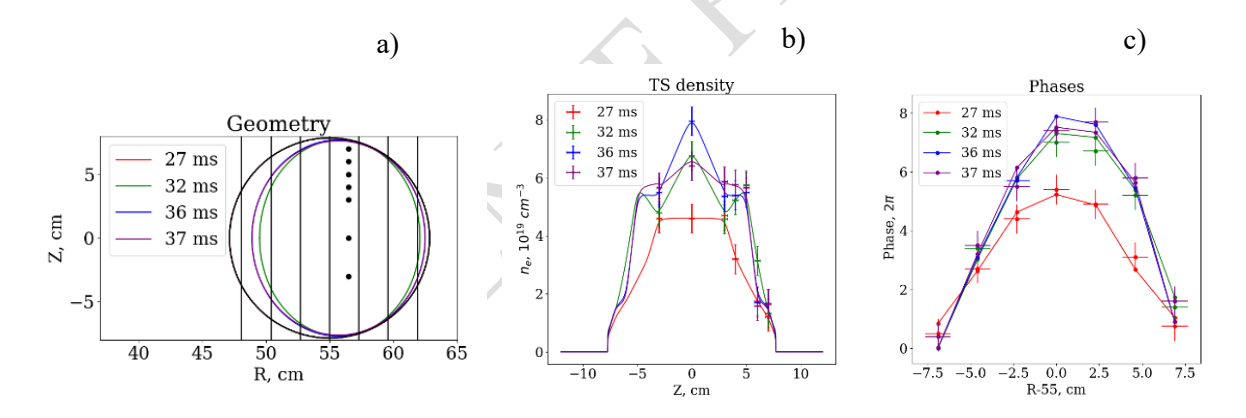


Fig. 2. (a) shows the plasma boundary for each case (27, 32, 36, and 37 ms), as well as the interferometer chords represented by black vertical lines; the regions observed by Thomson scattering diagnostics are marked with black dots. (b) displays the electron density along with TS experimental data points of height. (c) presents the interferometer phases as a function of the displacement of the observation chord relative to the major radius of the Vessel (R=0.55 m).

For 27 ms, the method of nested magnetic surfaces without deformation of the plasma column works well. For 32, 36, and 37 ms, a shift of 7 mm relative to the vessel center and elongation 1.2 is required, which determines the characteristic tilt of the interferometer phase. In this case, the plasma boundary barely touches the limiter at a major radius of 57.5 cm. Table 1 presents the parameters of the plasma boundary for each case. Fig. 3 shows separate graphs, depicted in Fig. 2.

TABLE 1.

time, ms	$\Delta$ – Shift, mm	a, cm	$\delta$ – triangularity	$\lambda$ - elongation
27	0	7.85	0	1
32	7	6.4	0	1.2
36	7	6.8	0	1.12
37	7	6.8	0	1.12

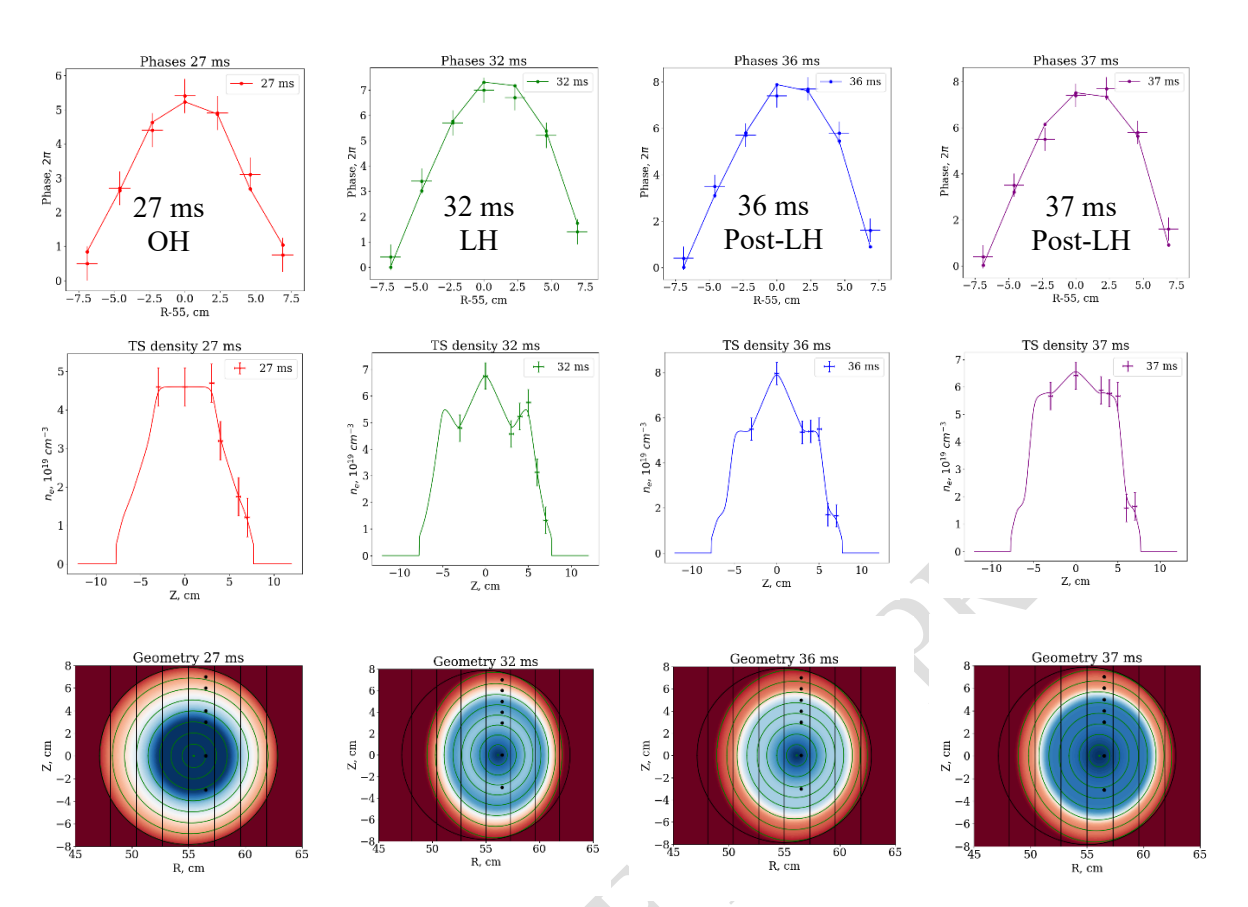
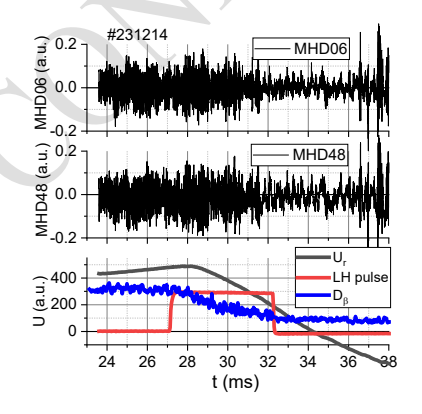


Fig.3. Profiles similar to Fig.3, but for each millisecond a separate graph. The density distribution throughout the entire plasma volume is indicated by color in the bottom row.

In the cases of 32–37 ms we observe a characteristic density profile shape with the formation of density "ears". The FT-2 tokamak has no particle sources inside the plasma, only gas puffing at the boundary. For this reason, the question arises about particle transport within the plasma—whether it is possible to form such a density profile shape with only a particle source at the plasma boundary.

Two possible causes for measured non-monotonic density profiles are considered in this paper: 1) plasma density suppression within the resonant cone of the LH wave due to the ponderomotive force, 2) formation of an internal transport barrier (ITB). Possible role of magnetic islands in the formation of the nonmonotonic density profile is not considered here due to the calculations of the relative change of the island width [6] during LH pulse, based on MHD probes measurements (Fig. 4a). These calculations demonstrated that the normalized widths of the  $m_1 = 2$  ( $WI_{norm}$ ) and  $m_2 = 3$  ( $W2_{norm}$ ) modes does not change during the LH pulse meanwhile after switching off LH power the widths of these modes decrease (Fig. 4b).

160



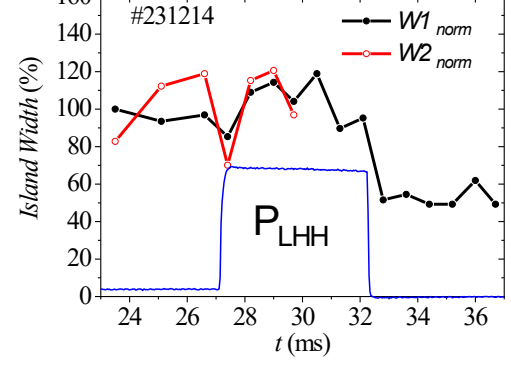


Fig. 4a. The signals from MHD probes 06 and 48 during LHH. horizontal equilibrium signal ( $U_r$ ), LH pulse and  $D_\beta$  line are shown

Fig. 4b. Dynamics of normalized island widths *W1* and *W2* (black and red) during LH pulse (blue) over time

#### 4. PONDEROMOTIVE EFFECTS AT THE LH HEATING. PLASMA CORE

The model of plasma density suppression during the propagation of a microwave in a resonant cone inside the plasma. The factor influencing the formation of non-monotonic density profile accompanied by formation of an additional maximum (and "ears") can be determined by the effect of the plasma density suppression [7] due to the ponderomotive force of the microwave pump wave propagating in the resonant cone.

According to theory [8], the microwave waves excited by the antenna form a "structure of the resonant cone type," which, following the total magnetic field, circulates around the torus in both the and toroidal and poloidal cross-sections. As it slowly penetrates deeper into the plasma, it reaches the point of linear conversion of the electromagnetic wave into a plasma mode.

Fig. 5 presents the results of modeling the propagation of the pump microwave wave. It shows the two-dimensional distribution of plasma density in the presence of the microwave beam  $^{\infty} \exp\left(-z^2/w_z^2\right)$ ,  $w_z = 4$  cm propagating strictly perpendicular to the magnetic field along the equatorial plane. Fig.s 5a and 5b show the two-dimensional distribution of plasma density during oblique propagation of the microwave beam at different segments in the toroidal direction. When measuring with TS diagnostics in a cross-section shifted by 180° along the major circumference (i.e., displaced by 190 cm from the point of pump wave injection), "ears" and, correspondingly, an additional maximum will be observed on the density profile. Since this effect is associated with additional gas injection through PV2, it may also be related to the appearance of components with higher refractive index  $N_z^{max} \sim 5$  in the pump wave spectrum compared to injection through PV1.

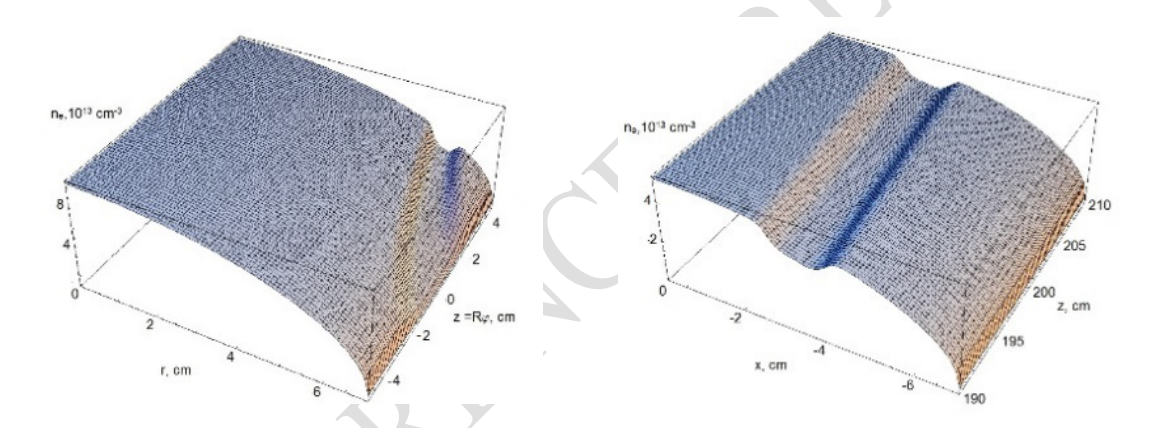


Fig. 5a. Oblique propagation of the microwave beam from the point of pump wave injection

Fig. 5b. For oblique propagation, the two-dimensional plasma density distribution is shown within the resonance cone in a region toroidally displaced by 180° along the major circumference (i.e., displaced by 190 cm) from the point of microwave beam injection.

## 5. PONDEROMOTIVE EFFECTS AT THE LH HEATING. PLASMA SOL

Another motivation regarding the significant influence of the ponderomotive force on the plasma arose from the probe measurements, which provided a plasma density drop in the SOL (scrape-off layer) near the grill during LHH in the PV2 case. Plasma parameters in the SOL region were measured using a movable (shot-to-shot) five-electrode Langmuir probe [9] (probe P3), located in a cross-section toroidally offset by 90° from the position of the LH antenna grill. Measurements of the radial profiles of  $n_e$  and  $T_e$  showed that during the LH pulse, the magnitude and gradient of  $n_e$  increase, accompanied by a decrease in the magnitude and gradient of  $T_e$ . These altered values persist for some time after the LH pulse ends. Such behavior of the parameters in the SOL is characteristic of the formation of a peripheral transport barrier, which is confirmed by measurements from other diagnostics. The SOL plasma density near the LH antenna was monitored by measuring the ion saturation current ( $I_{sat} \sim n_e T_e^{1/2}$ ) with the RF probe P2 (a metal pin). In this case, it was not used for receiving the RF signal but was instead connected in a single Langmuir probe circuit.

In contrast to the results obtained in measurements in the adjacent cross-section, a decrease in  $n_e$  was observed during the LH pulse,  $P_{RF} = 100 \text{kW}$  (an effect of plasma suppression near the antenna). A comparison of the  $I_{sat}$ 

[Left hand page running head is author's name in Times New Roman 8 point bold capitals, centred. For more than two authors, write AUTHOR et al.]

behavior, simultaneously measured in two toroidally separated cross-sections of the tokamak during gas injection through PV2 (#022124), is shown in Fig. 6.

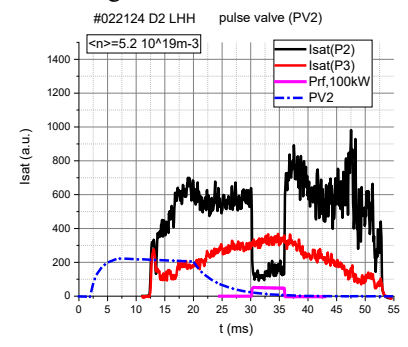


Fig. 6. Comparison of *I<sub>sat</sub>* collected by the RF probe (P2) and the toroidally displaced movable probe (P3). The dash-dotted line indicates the timing of the triggering pulse for the gas injection valve PV2.

A decrease in the edge plasma density in the frontal region of the radiating antenna can be explained by the influence of the ponderomotive force — a time-averaged force acting on a charged particle in an inhomogeneous, rapidly oscillating electromagnetic field. The spatial non-uniformity of the field amplitude causes drift motion towards the weaker field region (regardless of the charge sign). If the energy density of the electromagnetic field is significantly greater than the electron pressure in the edge plasma, there is a high probability of a power-dependent density decrease in the region in front of the antenna. A modification of the edge plasma parameters, apparently due to the ponderomotive force, was also observed on the ASDEX tokamak [10] in measurements taken far from the LH antenna.

The ponderomotive force acting on an electron can be expressed as:

$$f_{M} = -\nabla \Phi \tag{1}$$

 $\Phi$  is the potential of the averaged force acting on a single electron, which can be expressed as [11]:

$$n\Phi = \frac{\omega_{pe}^2}{\omega^2} \frac{E_{\parallel}^2}{8\pi} + \frac{\omega_{pe}^2}{\omega^2 - \omega_{ce}^2} \frac{E_{\perp}^2}{8\pi}$$
 (2)

where  $E_{II}$  and  $E_{\perp}$  are the parallel and perpendicular (with respect to the external magnetic field) components of the RF electric field, respectively, and  $\omega_{ce}$  and  $\omega_{pe}$  are the electron cyclotron and plasma frequencies.

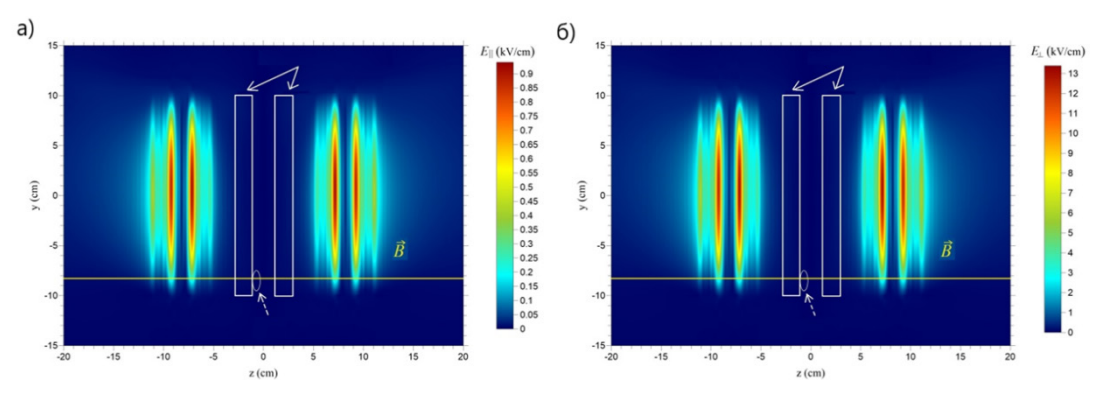


Fig. 7. The distributions of (a) the parallel and (b) the perpendicular components of the electric field in the plane where the probe is located. The yellow straight line is a magnetic field line with the magnetic induction vector **B**. The arrows indicate the grill waveguides. The small ellipse marks the position of the RF probe.

The results of LH wave modeling, performed using the Grill-3D code [12] for the experimental conditions, are shown in Fig. 7. It can be seen that even in the edge plasma, within the probe plane, two resonance cones of LH waves are formed. These are indicated by intense brown-red coloring and propagate in opposite directions along the toroidal coordinate z. The potential  $\Phi$  of the quasi-stationary ponderomotive force (2) reaches its maximum value  $\Phi$ \_max within these resonance cones and forms a pair of barriers for electron motion along the magnetic field.

Consequently, only electrons possessing kinetic energy exceeding the maximum value of the ponderomotive potential can penetrate into the relatively narrow region opposite the grill, located between the electric field maxima. The electron density in the region opposite the LH grill can be estimated as:

$$n \approx n_e \left( 1 - \int_{-v_m}^{v_m} \exp\left( -\frac{v^2}{v_{T_e}^2} \right) \frac{dv}{\sqrt{\pi}v_{T_e}} \right) = n_e \left( 1 - \frac{\delta n}{n_e} \right) = n_e \left( 1 - \operatorname{erf}\left( \sqrt{\frac{2\Phi_{max}}{m_e v_{T_e}^2}} \right) \right)$$
(3)

where  $v_m = \sqrt{\frac{2\Phi_{max}}{m_e}}$ , erf (...) is a probability function,  $n_e$  is the local plasma density far from the antenna, constant along the magnetic field line in the absence of LH waves, and  $v_{T_e} = \sqrt{\frac{2T_e}{m_e}}$ . This estimate does not account for the radial electron flow or the possibility of neutral gas ionization in the region opposite the grill.

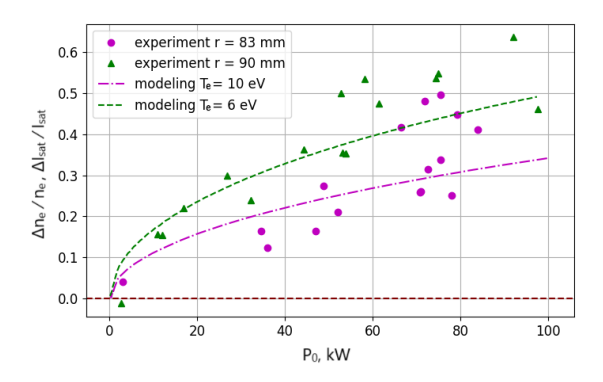


Fig. 8. Dependence of the experimental values of  $\Delta I_{sat}/I_{sat}$  and the calculated results for  $\Delta n/n$  on the LH power.

The results of the calculation using formula (3) for the relative density change  $\Delta n/n$  on the magnetic field line passing through the probe location, as a function of the total RF generator power for two values of electron temperature (6 eV and 10 eV), are shown in Fig. 8. This Fig. also shows the experimental values  $\frac{\Delta n}{n} \sim \frac{\Delta I_{sat}}{I_{sat}}$ , obtained at two radial positions of probe P2:  $r \approx 83$ mm (purple points) and  $r \approx 90$ mm (green triangles). The latter case corresponds to shifting the probe into a region with a lower  $T_e$  value. Unfortunately, it was not possible to experimentally obtain the radial  $T_e$  profile in this cross-section. Nevertheless, the Fig. 8 shows that the experimental results are consistent with the ponderomotive force model.

However, the fact that the non-monotonic density profile persists even after the switching off LH pulse calls into question the assumption that the ponderomotive force is the major factor influencing the effects observed during LHH. The ponderomotive effect could be a trigger for the plasma density profile transformation, but it is certainly not the primary cause.

## 6. ITB MODELING

Another possible reason of observed non-monotonic density profile relates to the hypothesis supposing the formation of a particle transport barrier in the inner plasma radii during LHH. This hypothesis was explored under the natural assumption of neutral particle influx from the plasma boundary.

[Left hand page running head is author's name in Times New Roman 8 point bold capitals, centred. For more than two authors, write **AUTHOR et al.**]

To investigate this, direct modeling of electron transport was performed using the diffusion equation in the ASTRA code [13].

$$\frac{1}{V'} \left( \frac{\partial}{\partial t} - \frac{\dot{B}_0}{2B_0} \frac{\partial}{\partial \rho} \rho \right) (V' n_e) + \frac{1}{V'} \frac{\partial}{\partial \rho} \Gamma_e = S_e, \tag{4}$$

Where the particle flux  $\Gamma_e$  is calculated using an equation that incorporates the diffusion coefficient  $D_n$ , pinch velocity  $C_n$  and other transport coefficients:

$$\begin{pmatrix}
\frac{\Gamma_{e}}{n_{e}} \\
\frac{q_{e}}{n_{e}T_{e}} \\
\frac{q_{i}}{n_{i}T_{i}} \\
V'G_{1}\frac{\mu_{0}j_{BS}}{B_{p}}
\end{pmatrix} = -V'G_{1}\begin{pmatrix}
D_{n} & D_{e} & D_{i} & D_{E} \\
\chi_{n}^{e} & \chi_{e} & \chi_{i}^{e} & \chi_{E}^{e} \\
\chi_{n}^{i} & \chi_{e}^{i} & \chi_{i} & \chi_{E}^{i} \\
C_{n} & C_{e} & C_{i} & 0
\end{pmatrix} \cdot \begin{pmatrix}
\frac{1}{n_{e}}\frac{\partial n_{e}}{\partial \rho} \\
\frac{1}{T_{e}}\frac{\partial T_{e}}{\partial \rho} \\
\frac{1}{T_{i}}\frac{\partial T_{i}}{\partial \rho} \\
\frac{E_{\parallel}}{B_{p}}
\end{pmatrix} (5)$$

The particle source was calculated using the NEUT code, which also took into account all ionization and recombination processes:

$$S_e = s_{ion}^{(e)} N n_e + s_{ion}^{(i)} N n_i - s_{rec} n_i n_e$$
(6)

As a result, to describe the experimentally measured electron density profile at 27 ms, the density diffusion coefficient shown in Fig. 9a possessing a sharp increase at the normalized minor radius of 0.6 must be used. At t=36 ms a diffusion coefficient with two transport barriers at normalized minor radii of 0.3 ( $q \sim 1$ ) and 0.8 ( $q \sim 2$ ) (Fig. 2) should be used.

For 32 ms, a simple linear pinch was necessary to produce the "ears" in the density profile. As can be seen from Fig. 9, the values of the pinch velocity selected linearly increasing to the periphery of the cord turned out to be ignificantly higher than the neoclassical Ware pinch velocity (pink line). It is possible that the transport of charged particles here was influenced by the ponderomotive mechanism associated with the propagating LH wave.

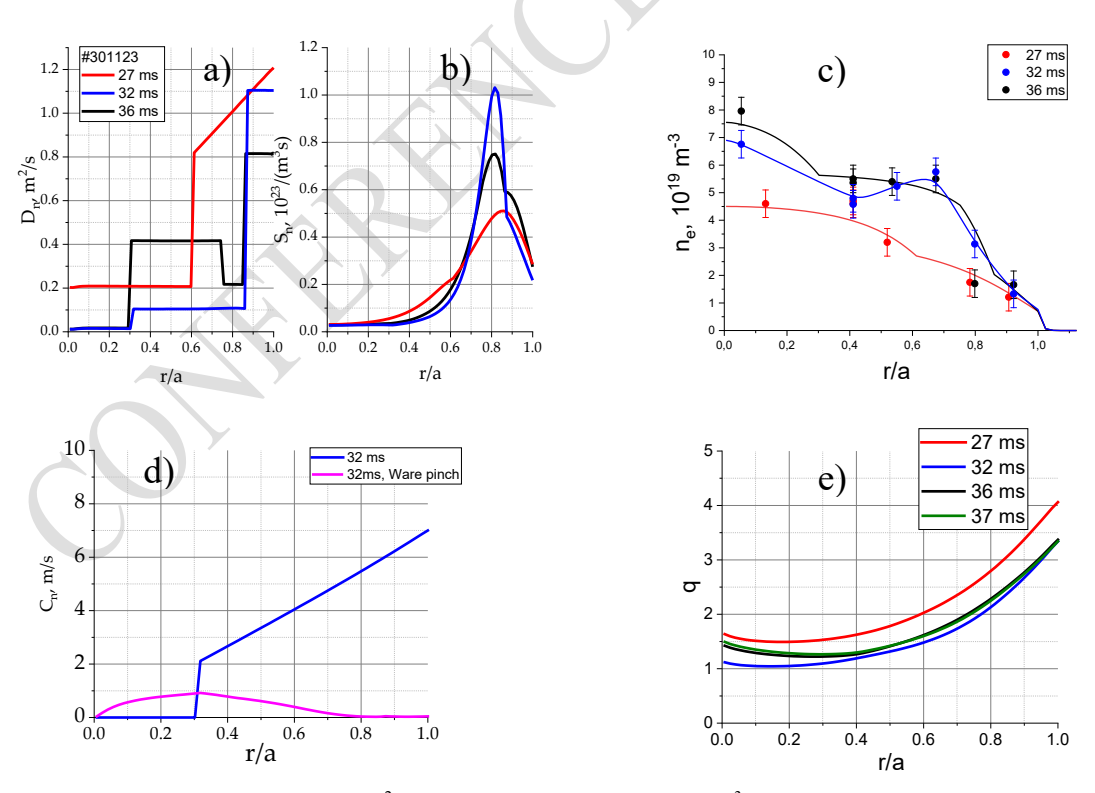


Fig. 9: (a) – diffusion coefficients D,  $m^2/s$ , (b) particle source intensity S,  $m^3/s$ ; (c) – electron density profiles, dots denote TS experimental values; (d) – pinch particle velocity  $C_n$ , m/s, for 32m, (e) – safety factor q.

#### 7. CONCLUSIONS

Thus, an increase in the efficiency of ion heating was observed when the working gas was injected through the grill port, leading to stabilization of the parametric decay instability of the lower hybrid wave [3, 4]. Additionally, the formation of a non-monotonic density profile during LHH was detected. An analysis of two possible factors causing this effect is carried out: ITB formation and ponderomotive forces. A more probable explanation is that the ponderomotive effect could be considered as a trigger for the plasma density profile transformation, but the ITB formation during LHH is more likely to explain the observed effects.

The modification of edge plasma parameters due to the ponderomotive force is expected to play a significant role in future large-scale facilities at high power levels, impacting the antenna-plasma coupling efficiency. It should be noted that, unlike the indirect evidence of a density decrease in the edge plasma in front of the antenna on the ASDEX tokamak [10], this study provides direct confirmation of this effect through measurements made in the vicinity of the grill.

#### ACKNOWLEDGEMENTS

The financial support of the Ioffe Institute state contracts № FFUG- 2021-0001 and № FFUG-2024-0028 is acknowledged.

#### REFERENCES

- [1] V.E. Golant, V.I. Fedorov. High-frequency methods of plasma heating in toroidal fusion devices (in Russian), (Energoatomizdat, M., 1986), pp. 69–96, 116–141
- [2] S.I. Lashkul, A.B. Altukhov, A.D. Gurchenko, et al., Technical Physics Letters, (2024), Vol. 50, No.3. pp. 73-76
- [3] S.I. Lashkul, A. B. Altukhov, A. D. Gurchenko et al., Plasma Physics Reports, (2020), Vol. 46, No. 9, pp. 863-873
- [4] C. Castaldo, A. Di Siena, R. Fedele et all. Nuclear Fusion 56 (2016) 016003
- [5] A.V. Sidorov et al., Technical Physics, 2022, Vol. 92, No. 4
- [6] H. R. Wilson (2006) Neoclassical Tearing Modes, Fusion Science and Technology, 49:2T, 155-163. https://doi.org/10.13182/FST06-A1115
- [7] A. Zabolotsky, H. Weisen and TCV Team. Plasma Phys. Control. Fusion 48 (2006) 369–383 doi:10.1088/0741-3335/48/3/003
- [8] A.G. Litvak, in Reviews of Plasma Physics, edited by M. A. Leontovich (Consultants Bureau, New York) (1986), vol. 10, p. 293
- [9] S.V. Shatalin, E.O. Vekshina, P.R. Goncharov, et al., Plasma Physics Reports, 2004. Vol. 30, No. 5, pp. 363-369
- [10] V.A. Petrzilka, F. Leuterer, F.-X. Soldner et al., Nucl. Fusion, 1991, Vol. 31, p. 1758. doi: 10.1088/0029-5515/31/9/014
- [11] V.I. Karpman, A.G. Shagalov J. Plasma Physics. 1982. V.27. P. 215. doi: https://doi.org/10.1017/S0022377800026544
- [12] M.A. Irzak, O.N. Shcherbinin Nucl. Fusion. 1995 V. 35 P. 1341. doi: 10.1088/0029-5515/35/11/I02
- [13] G. Pereverzev and P. Yushmanov, Report No. 5/98. (Max-Planck-Institut für Plasmaphysik, Garching, 1998)